Available online at www.sciencedirect.com
SCIENCE DIRECT®
Journal of Catalysis 219 (2003) 337–351
JOURNAL OF CATALYSIS
www.elsevier.com/locate/jcat

BiO_x clusters occluded in a ZSM-5 matrix: preparation, characterization, and catalytic behavior in liquid-phase oxidation of hydrocarbons

D. Dumitriu,[a] R. Bârjega,[a,b] L. Frunza,[b] D. Macovei,[b] T. Hu,[c] Y. Xie,[c] V.I. Pârvulescu,[a] and S. Kaliaguine [d,*]

[a] *University of Bucharest, Department of Chemical Technology and Catalysis, B-dul Regina Elisabeta 4-12, Bucharest 70346, Romania*
[b] *National Institute of Materials Physics, PO Box MG-7, RO-76900 Bucharest-Magurele, Romania*
[c] *Institute of High Energy Physics, Beijing Synchrotron Radiation Facility, PO Box 918, 100039 Beijing, People's Republic of China*
[d] *Université Laval, Département de Génie Chimique, Ste-Foy, PQ G1K 7P4, Canada*

Received 21 January 2003; revised 24 April 2003; accepted 13 May 2003

Abstract

A series of Bi-ZSM-5 containing 4.26, 5.54, and 6.64 wt% bismuth oxide was prepared by introducing Bi during ZSM-5 synthesis. For comparison, 5 wt% Bi (expressed as bismuth oxide)-impregnated ZSM-5 samples were also prepared. These samples were characterized by N_2 adsorption–desorption isotherms at 77 K, XRD, XPS, IR spectroscopy in the lattice vibration range and in the presence of chemisorbed pyridine and CO_2 and EXAFS. The characterization data confirmed the occlusion of bismuth oxide clusters in the zeolite pores. An intrinsic acidity due to bismuth oxide clusters was evidenced. This consisted, on one hand, in weak Lewis acid sites, ascribed to coordinatively unsaturated bismuth cations, and, on the other hand, in strong *Brönsted* acid sites, attributed to boundary Bi···O–Si linkages. These catalysts were tested in the liquid-phase oxidation of benzene, toluene, and cyclohexane using hydrogen peroxide as oxidizing agent. The results showed that Bi-ZSM-5 catalysts are more active than the reported titanium silicalites, but the efficiency of H_2O_2 use was quite small, an important part of this being nonselectively decomposed. A good selectivity was observed in cyclohexane oxidation.

Keywords: Occluded Bi oxide clusters; ZSM-5; XPS; XRD; EXAFS; *py* and CO_2-FTIR; Liquid-phase oxidation; Benzene; Toluene; Cyclohexane

1. Introduction

Oxidation of various organic substrates under mild conditions, particularly in the liquid phase, is of a great interest due to the desire for selective, low-energy consuming, and environmentally friendly processes. Reagents such as organic hydroperoxides or hydrogen peroxide were often used in these reactions, whereas the use of *titanium silicalites* with different topologies was widely reported. Twenty years ago, titanium-containing microporous solids exhibiting MFI [1–14] and MEL-type [15–18] structures were found to be very effective in such reactions. These studies were subsequently extended to larger pores solids that were appropriate for the oxidation of bulky substrates, such as Ti-Beta [19–24] and, more recently, Ti-mesoporous molecular sieves [25–33].

The remarkable activity of titanium silicalites has been attributed to tetracoordinated Ti(IV) sites that are isolated in a crystalline highly hydrophobic silica-like matrix [8,34–42]. The ability of Ti(IV) sites to change their environment from a tetra- to a hexacoordinated state during catalytic reaction, by interaction with substrates or solvent molecules, is considered to be essential in controlling their activity. Octahedral Ti(IV) incorporated in amorphous silica–titania mixed oxides (ETS) is inactive in such oxidation reactions [43, 44]. The requirements for the environment of the tetrahedral Ti(IV) site are different for epoxidation reactions which do not require a crystalline silica matrix [42,45]. The detection of the extraframework TiO_2 nanophases was studied for the synthesis and characterization of titanium silicalites [46–49], because of their undesirable activity in the nonselective H_2O_2 decomposition. Although *titanium silicalite* catalysts have been investigated extensively, some disadvantages of these catalysts exist. For example, the relatively

* Corresponding author.
E-mail address: serge.kaliaguine@gch.ulaval.ca (S. Kaliaguine).

0021-9517/$ – see front matter
doi:10.1016/S0021-9517(03)00216-1

complicated synthesis routes for avoiding precipitation of TiO_2 as a separate phase, which often acts as a catalyst poison in the subsequent oxidation reactions by hydrogen peroxide, and the small crystal size (0.1–10 μm) of micro- and mesoporous *titanium silicates* make it difficult to separate the reaction products, which may limit their applications.

Other elements such as V(V) [50–52], Sn(IV) [53,54], Cr(VI) [55], Zr(IV) [56], and W(VI) [57] have been immobilized in crystalline or amorphous silica matrices for the same purposes. The activity of these materials in liquid-phase oxidation has generally been correlated with the redox properties of these elements [54,55,58], or with structural effects caused either by their accommodation in silica walls by grafting or occlusion [52,56,57] or by isomorphous substitution [50,53]. A very important criticism made to these catalysts was the possible leaching of the active species. Very recently Hutchings and co-workers [59], using a 2.4 wt% Ti TS-1, confirmed that in several reaction media, Ti was not leached out. When, however, a triol, such as glycerol, is present simultaneously with hydrogen peroxide in the reactor, some leaching of titanium located at the outer surface of the TS-1 particles occurs.

Another particular effect in hydrocarbon oxidation in the liquid phase on zeolites is related to the role of Brönsted acid sites. Their presence, as noted for Y, mordenite, and ZSM-5 zeolites, may determine different pathways in hydrogen peroxide activation [60,61].

The synthesis of new materials with both high activity and selectivity in liquid-phase oxidation with hydrogen peroxide that also contain nonleachable species is of current interest. Zeolite-hosted oxides might be a solution in this sense. The aim of this study was to prepare and investigate a new kind of heterogeneous oxidation catalyst, namely a zeolite-hosted bismuth oxide. For such a purpose, Bi oxide species were inserted in the ZSM-5-type pores during hydrothermal synthesis. This study examined the structural, textural, and acid–base changes caused by the presence of bismuth in the zeolite pores. These materials were investigated as catalysts in the liquid-phase oxidation of highly stable organic substrates such as benzene, toluene, and cyclohexane. Bismuth is a well-known component of the mixed-oxide catalysts for gas-phase oxidations [62]. Also, the introduction of Bi in Pt or Pd-based catalysts has been reported to improve the catalytic performances for the selective oxidation of alcohols or aldehydes in aqueous solutions [63,64]. The same effect was investigated in oxidation of glucose to gluconic acid [65], of glycerol to dihydroxyacetone [66], of 1,2-propandiol into lactic acid [67], of glyoxal to glyoxalic acid [68], of α-hydroxyacids to α-ketoacids [69,70], of 1-methoxy-2-propanol [71], and of glyceric and tartronic acids [72,73]. The conclusion that emerges from these studies is that bismuth exhibits a promoter effect able to generate new active centers that adsorb the oxidizing (OH) species.

2. Experimental

2.1. Catalysts preparation

Bi-ZSM-5 samples were hydrothermally synthesized according to a classical ZSM-5 synthesis procedure [74,75] adding bismuth nitrate as the Bi source. All reagents used were of Merck grade. The gel composition was $3.2Na_2O \cdot (Al_2O_3, Bi_2O_3) \cdot 60SiO_2 \cdot 960H_2O$. A 0.01 mol mixture of pseudo-boehmite and bismuth nitrate previously dissolved in HNO_3 at moderate temperature (molar ratios Bi/Al of 0, 0.74, 1.18, and 1.48, respectively) was dissolved in 87 g water and mixed with 7.3 g H_2SO_4 (98%) and 8.3 g of tetrapropylammonium bromide solution thoroughly for 2 h (Solution A). Separately 41.8 g sodium silicate (ca. 27% SiO_2) was dissolved in 22 g water (Solution B) and 6.2 g NaCl in 25 g water (Solution C). Solutions A and B were then added in portions in Solution C under stirring, and the mixture was mixed for another 2 h. After aging at 170–180 °C for 72 h, in a teflon-lined autoclave, the crystals were separated from the mother liquor, washed with bidistilled water, and heated at 500 °C for 5 h, in an air stream. Following this procedure Bi-ZSM-5 zeolites containing 4.26, 5.54, and 6.64 wt% Bi_2O_3 were produced. These were denoted as Bi4.26, Bi5.54, and Bi6.64, respectively. All these samples were in the Na form. The chemical composition of the resulting zeolite materials corresponded to the molar Si-to-(Al + Bi) ratios given in Table 1. For comparison, a Na-ZSM-5 sample with a Si-to-Al molar ratio of 30:1 was also synthesized.

The protonated form of the parent zeolite was prepared by ion exchange with an aqueous solution of NH_4NO_3 (0.2 M) at 80 °C. After filtration, zeolites were calcined at 500 °C for 5 h.

A 5 wt% Bi-ZSM-5 was also prepared by both wet and dry impregnation of Na-ZSM-5. According to the first route, an aqueous solution of $Bi(NO_3)_3$, in a volume corresponding to the incipient wetness capacity of the Na-ZSM-5 parent zeolite was contacted with 2 g of this zeolite. After drying, the sample was calcined at 500 °C for 5 h. Dry impregnated 5 wt% Bi-ZSM-5 was obtained by the intimate mixing of $Bi(NO_3)_3$ salt with Na-ZSM-5 zeolite, for a prolonged time (6 h), followed by calcination at 500 °C for 5 h. These samples were denoted Bi5-wi and Bi5-di, respectively.

Table 1
Chemical composition of Bi-containing ZSM-5 samples

Sample	Bi (wt%)	Al (wt%)	Na (wt%)	Si (wt%)	Si-to-(Al + Bi) atomic ratio	Al-to-Bi atomic ratio	Al-to-Na atomic ratio
Bi4.26	4.26	0.73	0.62	43.1	32.5	1.33	1.0
Bi5.54	5.54	0.60	0.52	42.8	31.5	0.85	1.0
Bi6.64	6.64	0.57	0.49	43.0	28.9	0.66	0.99
Bi5-wi	5.05	1.26	1.08	39.7	20.2	1.91	0.99
Bi5-di	5.00	1.27	1.08	39.7	19.9	1.96	1.0

2.2. Catalysts characterization

The chemical composition of the catalysts was determined by inductively coupled plasma absorption spectroscopy after dissolution in HF, using an ICP-AES Spectro equipment. Crystallinity of the prepared samples was evidenced by X-ray diffraction (XRD) with a DRON-2 apparatus, using a Fe-filtered Cu-K_α radiation with a goniometer speed of 1°/min over the 2θ range of 6–66°.

N_2 adsorption–desorption isotherms were recorded at −196 °C, in the relative pressure range of 10^{-6}–0.99, with a Micromeritics ASAP 2000 equipment, after the samples were degassed at 200 °C for 12 h, at 10^{-4} Pa. The surface area was calculated according to the Langmuir model, for the relative pressure range of 0.01–0.05. The pore volume was calculated from the amount of nitrogen desorbed at relative pressure of 0.95. The micropore diameter was calculated according to the Horvath–Kawazoe formalism.

Infrared spectra were recorded with a Perkin–Elmer 180 spectrophotometer. Spectra in the lattice vibrations range were recorded for wafers of sample mixed with $BaCl_2$ in a Pyrex IR cell, with KBr windows. Spectra of adsorbed pyridine were recorded after degassing the pyridine excess or the weakly adsorbed species either at room temperature, at 150 or at 300 °C. To determine the basic sites, the infrared spectra were recorded in the presence of 10 Torr CO_2 after outgassing (10^{-3} mbar, at 300 °C for 10 h) the samples. The adsorption was carried out at room temperature.

X-ray photoelectron spectra were recorded using an XPS-7000 Rigaku (Al anode, 1486.6 eV), taking as internal standard for binding energies the C1s level at 284.8 eV.

The local environment of the Bi atoms in the catalyst structure was investigated by EXAFS spectroscopy at the Bi L_3 edge (13,419 eV). The absorption spectra were measured in the transmission mode at the Beijing Synchroton Radiation Facility (BSRF), beamline 4W1B. The incident X-ray beam was analyzed using a Si(111) double-crystal monochromator, with the higher harmonics removed by a slight detuning of the second crystal. The primary data were acquired in a range between 200 eV below and 950 eV above the Bi L_3 edge.

The absorption spectra were analyzed with in-house routines, in several steps: (i) the preedge background and postedge structureless component ("atomic" absorption) were fitted by polynomials and cubic splines, respectively, and subtracted from the spectra; the EXAFS function $\chi(k)$ (k = photoelectron wave-vector) was calculated from the remaining oscillations, normalized by the atomic absorption; (ii) EXAFS was Fourier-transformed, resulting in a radial quasi-distribution, with maxima corresponding to the neighboring shells of the Bi atoms; (iii) the first maximum of the Fourier transform (FT) was isolated by a window function and backtransformed into the k-space; this provided the contribution of the closest neighbors to EXAFS, filtered out of the experimental spectrum; (iv) the filtered EXAFS was nonlinearly fitted, to derive the local Bi environment: the number of the nearest neighbors (N), the mean interatomic separation (R), and the distance-mean-square fluctuation (σ^2) around R [76,77].

The EXAFS standards (photoelectron backscattering amplitudes, phase shifts, amplitude losses by shake up/off processes, and inelastic scattering) were experimentally determined by measurements on α-Bi_2O_3.

TEM/EDX data were collected using a Philips EM430 microscope operating at 400 V equipped with an Oxford EDS detector.

2.3. Catalytic tests

Catalytic tests were carried out in a glass reactor (batch type) equipped with refrigerent, under vigorous magnetic stirring. The reaction temperature ranged between 50 and 90 °C. Benzene, toluene, and cyclohexane were used as test molecules. Oxidations were performed with H_2O_2 (30 wt% aqueous solution) for a H_2O_2/hydrocarbon molar ratio of 1:1. Typical experiments were carried out for 90 min using 0.1 g catalyst and 120 mmol of hydrocarbon. After reaction, the catalyst was separated by filtration *at the reaction temperature*. In order to check for the metal leaching the mother liquor was kept under reaction conditions for another 90 min. The mother liquor was then analyzed for Bi using ICP-AES. The analyses of the reaction products were performed in a gas chromatograph (Hewlett Packard GC 5710A/30 A) coupled to a ECD 18713A and equipped with a 4 m × 1.8 mm packed column of Carbowax 20M on Chromosorb W-HP. The products were identified by GC-MS (Hewlett Packard MS-5988). The H_2O_2 conversion was established by iodometric titration. The efficiency of H_2O_2 transformation was calculated as [moles of H_2O_2 utilized for oxy-functionalization of hydrocarbons/moles of H_2O_2 transformed] × 100. It was considered that oxofunctionalization of hydrocarbon to alcohol needs one H_2O_2, to ketone two H_2O_2, and to carboxylic acid three H_2O_2 molecules.

3. Results

3.1. Chemical composition and textural characterization

The starting gel contained the same Si-to-(Al + Bi) molar ratio, i.e., 30, for all the synthesized zeolites. Chemical analysis of the resulting materials showed different values depending on the Bi content (Table 1). This ratio slowly decreased with the increased Bi content, from 32.5 (for Bi4.26) to 28.9 (for Bi6.64%). Al-to-Bi molar ratios were also different from those in the gel. Al-to-Na molar ratios were very close to 1 for all the prepared samples.

For all investigated samples, N_2 adsorption–desorption curves at −196 °C corresponded to Langmuir-type isotherms. The surface areas and the pore volumes of these

Table 2
Textural properties of Bi-containing ZSM-5 samples

Sample	Surface area (m^2/g)	Pore volume (cm^3/g)
Na-ZSM-5	435	0.18
Bi4.26	410	0.17
Bi5.54	359	0.15
Bi6.64	280	0.1
Bi5-wi	210	0.07
Bi5-di	157	0.06

samples are given in Table 2. For hydrothermally synthesized Bi-ZSM-5 samples, an important decrease in the surface area with increasing bismuth content was observed. This decrease was accompanied by a decrease in the pore volume. No modification of the pore diameter was determined as a consequence of the bismuth loading, since the pore diameter, as calculated with the Horwath–Kawazoe formalism, was very close to 5.8 Å for all samples. The *t*-plot analysis did not indicate the formation of mesopores as a consequence of the increase in Bi loading.

Wet and dry impregnated Bi-ZSM-5 samples were characterized by a strong decrease in surface area and pore volume as compared to the parent Na-ZSM-5 sample.

3.2. XRD

The diffraction patterns of the calcined samples are presented in Fig. 1. Except for Bi6.64, the only one phase detected was that of the ZSM-5 zeolite (MFI structure type) [78]. For Bi6.64, the presence of additional phases like α-quartz and eulytite ($Bi_4(SiO_4)_3$, ASTM 33-215) was also evidenced.

Taking the Na-ZSM-5 sample as a reference, we evaluated the crystallinity of the Bi-containing zeolites from the intensity of the typical MFI peaks 501, 051, 151, 303, and 133, following a usual procedure [79–82]. The results are presented in Table 3. These show a decrease in crystallinity due to the presence of Bi. The low value associated with Bi6.64 is in direct relation to the presence of extra phases.

No expansion of the volume cell was observed for the Bi-ZSM-5 samples compared to the Na-ZSM-5 samples. This suggests that Bi^{3+}, as expected due to its very high ionic radius, did not isomorphously substitute the Al^{3+} in framework position. Bi is found inside the channel system or deposited on the external surface of the crystal, *where* even a crystalline phase could be formed as is the case for Bi6.64 (see below).

The low-angle XRD intensities are particularly sensitive to the presence of any species inside the channels [83–86]. As the atomic scattering factor of Bi is almost 8 times higher than that of Na [87] such a behavior should be reflected in the structural factor and, consequently, in the XRD intensity. This may explain the decreased intensities of the low-angle peaks of the Bi-ZSM-5 samples. The I_{101}/I_{501} ratio might be correlated to the Bi content inside the MFI channels system, since low values of this ratio are related to increased

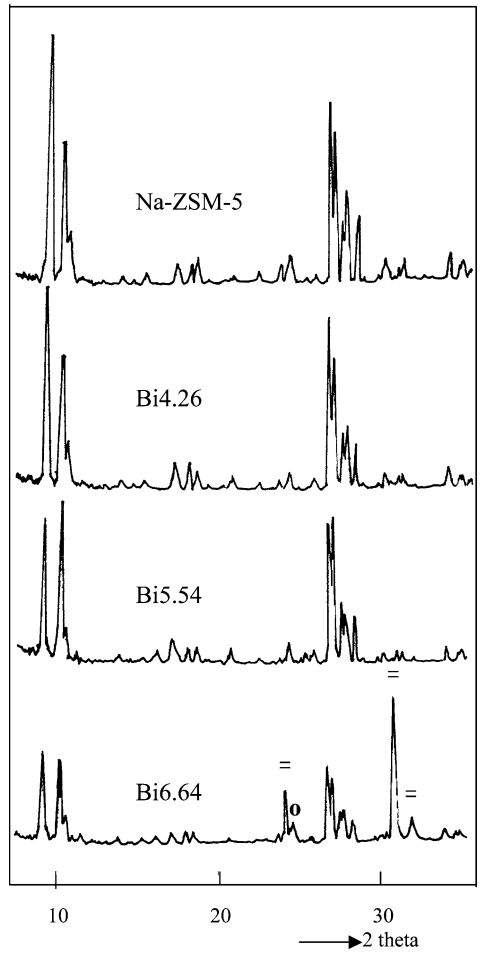

Fig. 1. XRD patterns of Na- and Bi-ZSM-5 zeolites.

Table 3
XRD representative data for synthesized Bi-ZSM-5 samples

Sample	Crystallinity (%)	I_{101}/I_{501}
Na-ZSM-5	100	1.45
Bi4.26	85	1.10
Bi5.54	80	0.99
Bi6.64	41	1.21

Bi content. Table 3 gives these intensity ratios. From this analysis, it results that for the hydrothermally prepared Bi-ZSM-5 samples, Bi5.54 contains the largest amount of Bi inside the channels, and Bi6.64 the lowest one. This may suggest for Bi6.64 the formation of an extraframework Bi-crystalline phase, very probably segregated on the external surface of the zeolite particles.

3.3. TEM/EDX analysis

TEM analysis of Bi4.26 and Bi5.54 indicated a typical ZSM-5 topography (Fig. 2a). The shape of the Bi6.64 particles was different, corresponding to more elongated crystals (Fig. 2b). EDX patterns yielded composition results in agreement with chemical analysis, indicating, for example,

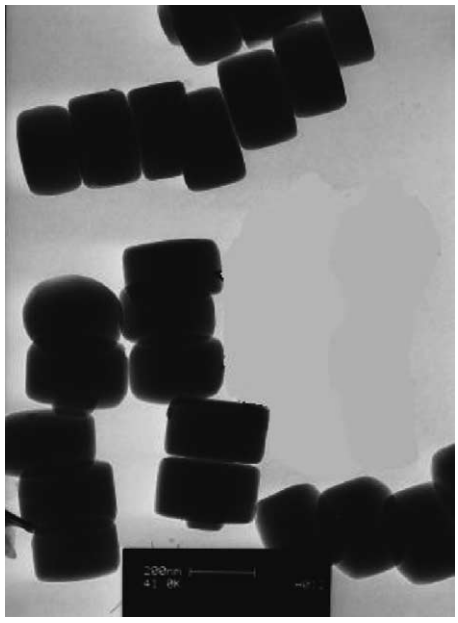

(a)

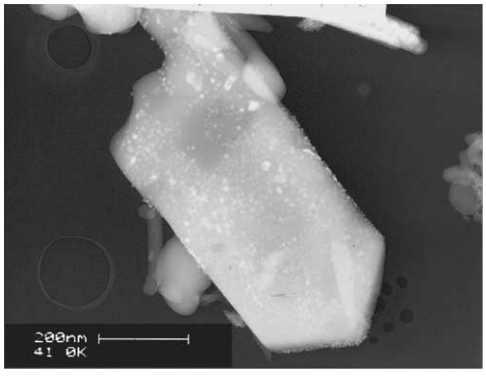

(b)

Fig. 2. TEM of Bi5.54 (a) and Bi6.64 (b).

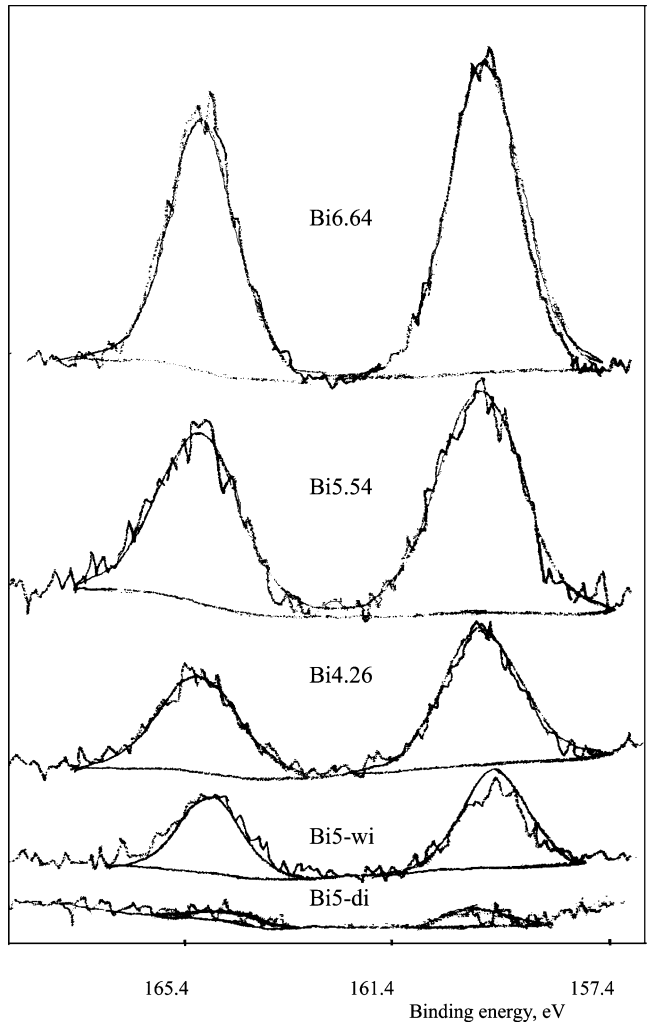

Fig. 3. XPS spectra of Bi-ZSM-5 zeolites in the region of Bi(4f).

Table 4
EDX atomic composition of the investigated catalysts

Catalyst	%Na	%Al	%Si	%Bi	%O	Si/(Al + Bi)
Na-ZSM-5	1.20	1.46	44.1	0	52.4	30.2
Bi4.26	0.79	0.73	41.5	0.51	55.9	33.4
Bi5.54	0.64	0.61	42.2	0.70	55.3	32.2
Bi6.64	0.54	0.53	42.4	0.82	55.2	31.4

comparable Si/(Bi + Al) ratios (compare Tables 1 and 4). In addition, Fig. 2b shows a population of microcrystals on the surface of the Bi6.64 particles which may correspond to segregated bismuth oxide.

3.4. XPS characterization

Representative XPS spectra are shown in Fig. 3. Binding energies of the $Bi4f_{7/2}$ level varied over a small range (Table 5), indicating no significant differences of the bismuth oxidation state in the investigated samples. These values should be compared to 159.8 eV, corresponding to the $Bi4f_{5/2}$ level in pure Bi_2O_3 [88].

Table 5
Surface composition of Bi containing ZSM-5 samples analyzed by XPS

Sample	Binding energies (eV)			Chemical	XPS
	Bi ($4f_{7/2}$)	Al (2p)	Si (2p)	(Si + Al)-to-Bi ratio	(Si + Al)-to-Bi ratio
Bi4.26	159.8	74.4	103.3	77.0	21.7
Bi5.54	159.8	74.9	103.3	59.1	17.5
Bi6.64	159.6	74.5	103.6	48.6	10.4
Bi5-wi	159.5	74.9	103.4	60.9	35.8
Bi5-di	159.8	74.7	103.3	61.2	235.5

Comparative chemical and XPS (Si + Al)-to-Bi ratios are also given in Table 5. Hydrothermally synthesized samples exhibit a superficial enrichment in bismuth. For the wet impregnated sample, comparing these ratios indicates also a Bi-enriched surface but less so than the hydrothermally synthesized samples which may suggest a better migration of bismuth inside the zeolite pores. For the dry impregnated sample, the XPS ratios should be interpreted with caution

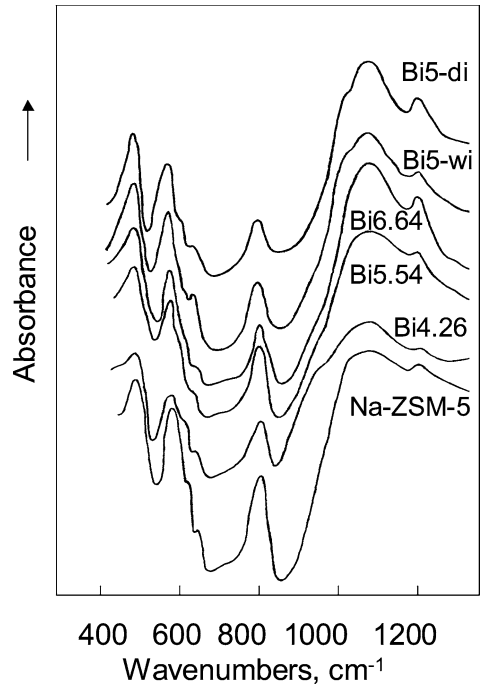

Fig. 4. FTIR spectra of the investigated zeolites in the framework region.

because some agglomerates of Bi oxide may strongly affect these results, part of Bi being XPS hidden.

3.5. Infrared spectra

3.5.1. Spectroscopy in the lattice vibration range

IR lattice vibration spectra were used to asses the influence of bismuth on the zeolite framework in ZSM-5 samples. Representative spectra are shown in Fig. 4. The main peaks at 450, 550, 800, and 1100 cm^{-1} have the general assignment given by Flanigen et al. [89] for the vibrational modes of zeolite framework to the bending of the TO_4 tetrahedra, to the structurally sensitive double five-membered ring (D5R) vibration, and to the symmetric and asymmetric stretching vibrations of the T–O–T linkages, respectively. The D5R vibration band at 550 cm^{-1} has two shoulders at 585 and 620 cm^{-1}, as expected for the structure of the pentasil family. The broadening of this D5R absorption for Bi-ZSM-5 samples as compared with the parent ZSM-5 sample is most probably due to the lattice distortion caused by bismuth oxide clusters in the pores (Bi^{3+} cation being three times larger than Si^{4+}).

Moreover, the ratio A_{550}/A_{450} (where A_{550} and A_{450} are the absorbance values corresponding to the bands at 550 and 450 cm^{-1}, respectively), known to indicate the sample crystallinity, seems to decrease when the Bi content increases (Table 6), even though some factors that affect this ratio, such as the phase content and the crystallinity, differ. As a consequence, the IR spectra in the lattice range are more evidence of the Bi disruptive influence on the zeolite framework as the bismuth content increases.

Table 6
A_{550}/A_{450} ratios and normalized absorbance values for *py* species adsorbed on Brönsted (*py*-B) and Lewis acid sites (*py*-L) at 150 °C

Sample	A_{550}/A_{450}	*py*-B (absorbance/g)	*py*-L (absorbance/g)
H-ZSM-5	0.74	10.0	4.2
Na-ZSM-5	0.74	0	4.3
Bi4.26	0.62	3.9	4.2
Bi5.54	0.65	6.3	6.7
Bi6.64	0.52	3.1	10.1

On the other hand, since silicon and bismuth are sufficiently different in atomic weight to change the reduced mass of the harmonic oscillator as compared to the silicon–aluminum pair, separate Si–O–Si and Si–O–Bi stretching bands are expected [89]. However, the spectra show no peak that might be attributed to the symmetric stretching of Si–O–Bi vibrations. Instead, Fig. 4 shows additional absorptions as compared to Na-ZSM-5, such as the large peak near 950 cm^{-1}, which is generally attributed to the stretching vibrations of a SiO_4 tetrahedron perturbed by the presence of a metallic ion or of a hydroxyl group (–$(SiO)_3$Si–OH or Bi–OH), where the latter group appeared when Bi oxide was introduced in zeolite pores [90,91]. In the spectra of Bi-ZSM-5 samples (Fig. 4), the large shoulder around 960 cm^{-1} may be assigned to an ensemble –$(SiO)_3$Si–O–Bi, since neither impregnated samples nor pure MFI samples exhibit such absorptions. The band tends to diminish in the following order: Bi4.26 > Bi5.54 > Bi6.64. For the impregnated zeolites, an additional shoulder at 1060 cm^{-1} was observed. However, its nature is still unclear. In the case of Co-ZSM-5 samples, a similar band was controversially assigned to the presence of large cobalt oxide particles or to asymmetric stretching of Si–O–Co vibrations [92].

3.5.2. IR spectroscopy in the presence of adsorbed pyridine

The FTIR spectra of pyridine adsorbed on Bi catalysts are illustrated for a Bi5.54 sample in Fig. 5. The spectra show the typical absorption bands assigned to the 8a and 19b vibration modes of adsorbed-*py* forming Lewis-type adducts (*py*-L, *py*-M) with bands at 1603–1618 and 1450 cm^{-1}, and to the 19b mode of Py in interaction with Brönsted acid sites (*py*-B) as the band at 1541 cm^{-1}. The intensity of these bands changes according to the chemical composition of the catalysts and the activation conditions. The band at 1491 cm^{-1} is assigned to *py* adsorbed on both Lewis and Brönsted acid sites [93,94].

As noted above, the peak at 1541 cm^{-1} corresponds to the protonic acidity. The spectra of Bi4.26 and Bi5.54 also show a shoulder located at 1555 cm^{-1}. This may correspond to a Brönsted acid site generated by the Bi species, which has been previously reported for Bi-exchanged X zeolites [95]. The peak at 1603 cm^{-1} is related to bismuth oxide clusters and may also correspond to *py*-M adducts formed onto Bi/BiO^+ species. The intensity of this band de-

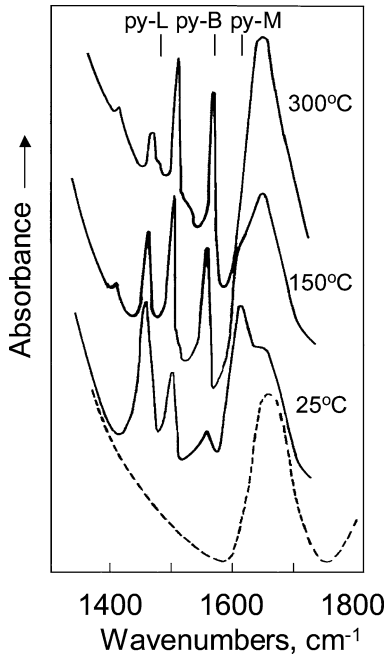

Fig. 5. *py*-FTIR spectra of a Bi5.54 sample after outgassing at different temperatures; the dashed line represents the background.

creases quickly when the desorption temperature increases from room temperature to 150 °C.

The normalized absorbance values (Table 6) show a different concentration of the acid sites depending on the Bi loading. All samples adsorbed less *py* than the protonic form of the parent ZSM-5 zeolite. There are some differences regarding the ratio of the peak area of the bands due to the 19b vibration mode of *py*-L species and *py*-B species, respectively. The samples H-ZSM-5 and Na-ZSM-5 are given as references. The data in Table 6 indicate that, compared to the parent Na-ZSM-5 sample, the three Bi-ZSM-5 show an enhanced concentration of both Brönsted and Lewis acid sites. A maximum in Brönsted acid concentration is observed for Bi5.54 whereas Bi6.64 shows the highest content in Lewis acid sites. It is worth noting that the spectra recorded for the two impregnated Bi-ZSM-5 zeolites showed almost no *py* adsorption. Since a low capacity was found for pyridine chemisorption onto Bi_2O_3 in various oxide environments [96], the impregnated samples might have contained (low dispersed) oxidic Bi phases.

In conclusion, the presence of Bi clusters in the pores of the ZSM-5 generated both Brönsted and Lewis acidity. Increasing the Bi content to 5.54 wt% led to two Brönsted sites (responsible for 1541 and 1555 cm^{-1} bands) that may be associated with the formation of Si–O–Bi bridges. The Lewis acidity may correspond to low coordination Bi sites at the surface of Bi clusters. A further increase in the Bi loading yields a decrease in Brönsted sites and an increase in Lewis sites, that suggests a formation of a bulkier Bi oxide phase, and may correspond to the observed disruption of the zeolite framework.

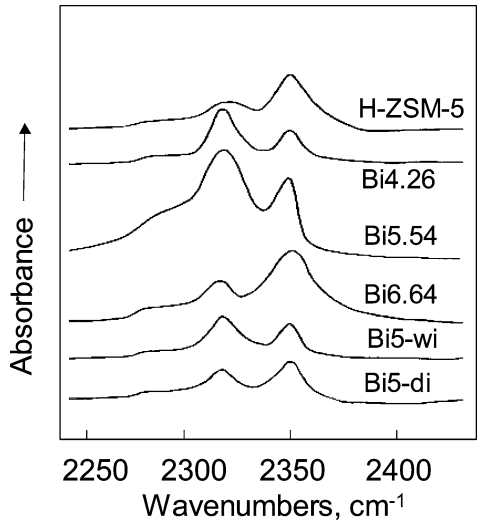

Fig. 6. CO_2-FTIR spectra of the investigated zeolites (room temperature).

3.5.3. IR spectroscopy in the presence of adsorbed CO_2

Carbon dioxide is a suitable probe molecule for revealing both the surface basicity and acidity [97]. Acidity information results from the adsorption of carbon dioxide on the coordinatively unsaturated (cus) cations of the surface through oxygen lone pairs. The corresponding IR absorption bands appear in the range of 2250–2450 cm^{-1} [98–107]. Carbon dioxide can also interact with basic sites (some OH species, cus O^{2-}, or cus anion–cation couples) yielding various types of carbonate-like species that have absorption bands in the spectral range of 1200–1700 cm^{-1} [108].

It is especially significant that no IR band was observed in the spectra of the three Bi-ZSM-5 in the spectral range of 1200–1700 cm^{-1}, indicating that these materials bear no basic sites.

Fig. 6 gives the spectra in the 2250–2450 cm^{-1} region, recorded for carbon dioxide adsorbed at room temperature on the investigated samples. Two bands are observed that disappear entirely upon evacuation at 100 °C. They correspond to the CO_2 molecule weakly interacting with the Lewis centers on these samples. A weak band also appears at about 2275 cm^{-1} that might be assigned to the asymmetric *stretching of adsorbed CO_2 containing the natural ^{13}C isotope*. The evolution of the relative intensities of the two bands (2315 and 2350 cm^{-1}) with the Bi content and preparation procedure does not allow a more clear assignment. However, the two samples which contain Bi clusters (Bi4.26 and Bi5.54) show a clearly enhanced contribution of the 2315 cm^{-1} band, suggesting a particular type of interaction between CO_2 and the Lewis acid sites on the Bi clusters.

3.6. EXAFS

3.6.1. α-Bi_2O_3

Since the nearest neighbors of bismuth in the structure of the investigated catalysts are most likely oxygen atoms, the choice of α-Bi_2O_3 as a standard compound for the EXAFS

analysis seemed to be a suitable one. However, its complicated structure, with the closest O neighbors spread over a wide range of distances around the Bi atoms, makes the inference of the EXAFS standards less straightforward. The adopted approach is briefly discussed below.

The crystal lattice of α-Bi_2O_3 has a monoclinic, low-symmetry structure, belonging to the space group $P2_1/c$ [109]. Its large unit cell ($a = 5.8496$ Å, $b = 8.1648$ Å, $c = 7.5101$ Å, $\beta = 112.98°$) contains four molecules, with the Bi and O atoms distributed over two and three types of nonequivalent sites, respectively.

The resulting pair distribution around a central, mean Bi atom, averaged over its two specific sites, is shown in Fig. 7a. A group of 11 Bi–O distances is clearly distinct in the range 2.13–2.79 Å of the distribution, corresponding to the nearest oxygen neighbors of the Bi atoms. A small-distance detail (Fig. 7b) shows a further differentiation, between a subgroup of 6 distances, in the range 2.13–2.28 Å, and another one of 5 distances in the wider range 2.42 to 2.79 Å. This suggests that the asymmetric radial distribution of the nearest neighbors might be approximated by two neighboring shells of 3 O and 2.5 O atoms, at unique distances corresponding to the mean values of the two subgroups (2.20 and 2.59 Å, respectively).

To check this hypothesis, the first main maximum in the Fourier transform of $k^3\chi(k)$ spectrum of α-Bi_2O_3 (Fig. 8a) was isolated and backtransformed into the k-space, to obtain

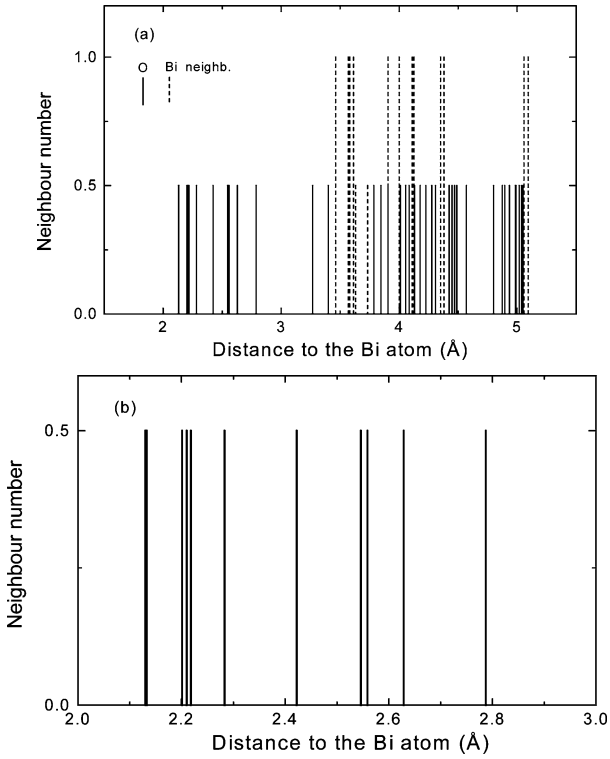

Fig. 7. (a) Pair distribution in the structure of α-Bi_2O_3, around a mean Bi atom, averaged over the two nonequivalent Bi sites in the unit cell. (b) Short-distance detail of the distribution, corresponding to the nearest O neighbors of the mean Bi atom.

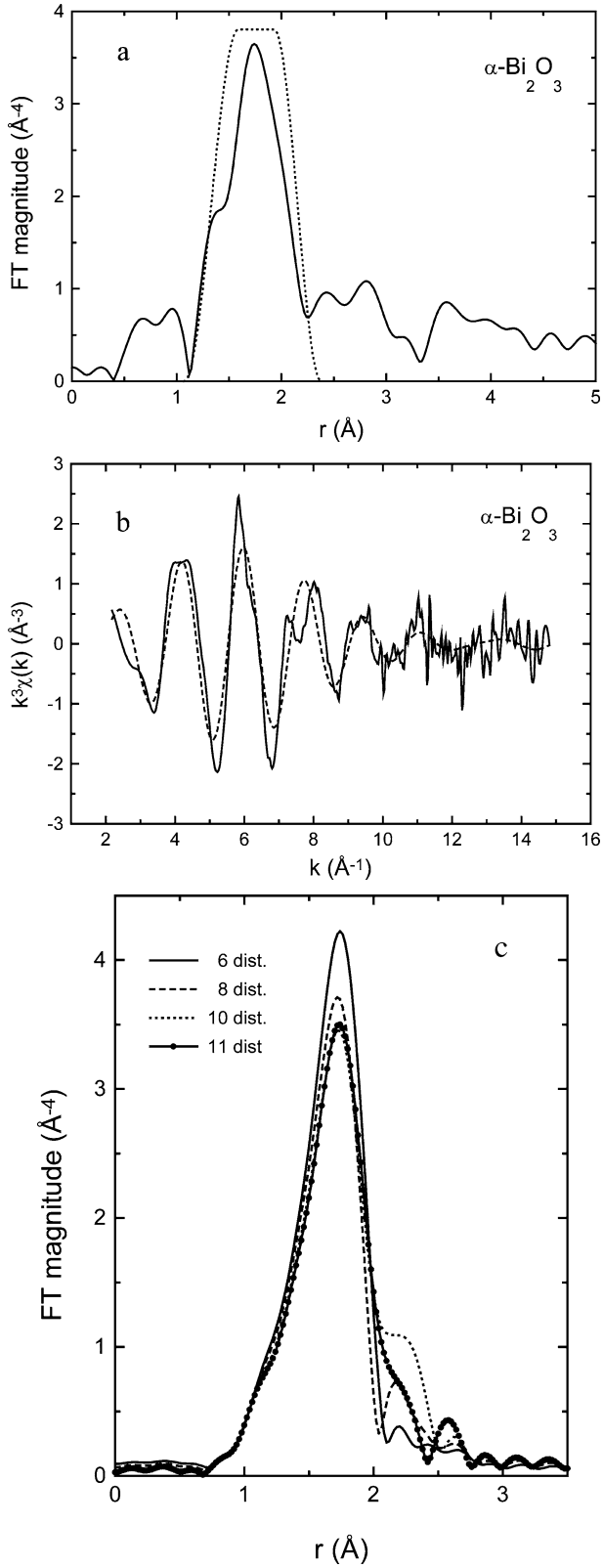

Fig. 8. EXAFS results for α-Bi_2O_3. (a) Fourier transform of $k^3\chi(k)$ spectrum of α-Bi_2O_3 and the filtering window (dots) used to isolate the first main maximum; (b) experimental $k^3\chi(k)$ spectrum (solid line) of α-Bi_2O_3 and the filtered spectrum (dashed line) corresponding to the contribution of the nearest neighbors; (c) Fourier transforms of the simulated $k^3\chi(k)$ spectra of α-Bi_2O_3, calculated with various numbers of Bi–O distances.

the separate contribution to EXAFS of the local Bi environment (Fig. 8b).

Attempts to fit the filtered spectrum with two neighboring shells, using theoretical EXAFS standards calculated by the *FEFF6* code [76,77], were unsuccessful. Rather surprisingly, the fit with a unique shell was much more convincing. It found a number of 3.0–3.3 O neighbors at a distance of 2.26 Å. This shows that the closest surrounding of bismuth can be satisfactorily approximated by a unique shell. It could be tempting to describe this shell by an average over the shortest six Bi–O distances (3 O neighbors at 2.20 Å). However, it seems more reasonable to assume the first maximum of FT as being contributed by a number of Bi–O pairs intermediate between 6 and 11, with corresponding mean distances of 2.20 and 2.37 Å, respectively.

In order to establish this number, the EXAFS spectrum of α-Bi_2O_3 was successively simulated with an increasing number of distances in the range 6 to 11. The EXAFS standards were individually calculated for each Bi–O distance (with Bi as absorber and O as backscatterer) by the FEFF6 code, with the amplitude reduction factor $S_0^2 = 0.774$, characteristic of Bi [110]. The EXAFS spectra were afterward calculated, by assuming a constant σ^2 factor, set to 0.005 $Å^2$, over all the contributing distances.

The FTs of the simulated spectra are represented in Fig. 8c. One can see that by increasing the number of contributing distances in the range from 6 to 10, the amplitude of the main maximum, at about 1.74 Å, gradually diminishes, at the same time with the enhancement of a second, smaller peak at about 2.2 Å. The 11th distance induces a change: the peak at 2.2 Å is reduced to a shoulder, while another peak becomes visible at about 2.6 Å.

By comparing these results with the FT of the experimental spectrum (see Fig. 8a), one finds a reasonable similarity to the 10-distance simulation, provided that the small peak at 2.4 Å in the experimental FT is taken into consideration. This was done by a corresponding widening to the right of the initial filtering window in Fig. 8a.

The new-filtered EXAFS was therefore assigned to a unique shell of nearest neighbors, consisting of 5 O atoms at 2.33 Å. This allowed derivation of the experimental EXAFS standards, subsequently used in the analysis of the catalysts.

One must finally remark that approximating the nearest neighbor distribution by a unique shell is a crude estimate for an accurate description of the α-Bi_2O_3 structure. However, it is reasonably adequate for the goal of this work, which was to infer EXAFS standards characteristic of the Bi–O distances in the catalyst structure.

3.6.2. Bi catalysts

The absorption spectra of the Bi catalysts, after the subtraction of the preedge background, are shown in Fig. 9. Although the primary spectra were measured up to about 950 eV above the Bi L_3 edge, their further analysis (Fourier transformation and nonlinear fit) was limited to energies lower than 630 eV above the edge, due to glitches in the spectra beyond this limit.

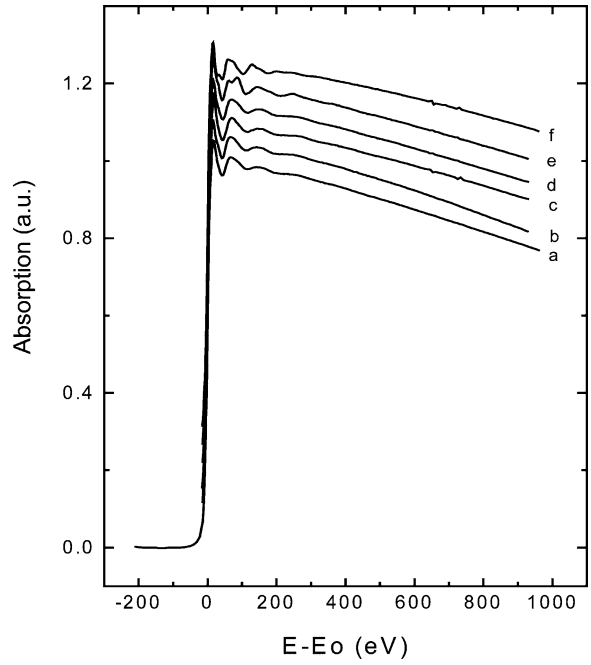

Fig. 9. Absorption spectra of catalysts with Bi concentration (wt%): Bi4.26 (a); Bi5-wi (b); Bi5-di (c); Bi5.54 (d); Bi6.64 (e). Spectrum f belongs to α-Bi_2O_3. The spectra were represented with respect to the photoelectron energy (E = energy of the incident x photons, E_0 = energy of the Bi L_3 edge) and were displaced on the vertical for the sake of clarity.

The Fourier transforms of the $k^3\chi(k)$ spectra are represented in Fig. 10a. The main maximum at about 1.65 Å describes the closest oxygen surrounding bismuth in the catalyst structure. All the other maxima are strongly dampened for the samples Bi4.26, Bi5.54, Bi5-wi, and Bi5-di, which proves a high structural disorder beyond the nearest neighboring shell. However, for the sample Bi6.64 (Fig. 10a, spectrum e), two intense maxima are distinct at 2.98 and 3.80 Å, related to a medium-range order, extended at relatively large distances, instead of the short-range order in the other samples. Therefore, a crystalline structure is locally developed around the Bi atoms in this sample.

The main maximum in the FTs was isolated, as previously described, and backtransformed into the k-space. The so-filtered spectra (Fig. 10b) define the separate contribution to EXAFS of the nearest O neighbors. It was successively fitted with one and two neighboring shells, using the experimental EXAFS standards. However, only the one-shell model yielded physical results, given in Table 7. The Bi atoms are most closely surrounded by about 3 O atoms at a distance of about 2.2 Å. The number of the nearest neighbors, as well as the interatomic distance, could indicate a local Bi environment very close to that in the structure of α-Bi_2O_3, confined to the shortest six Bi–O distances ($N = 3$, average $R = 2.20$ Å). However, as shown by the negative values of $\Delta\sigma^2$, the oxygen configuration around Bi atoms is

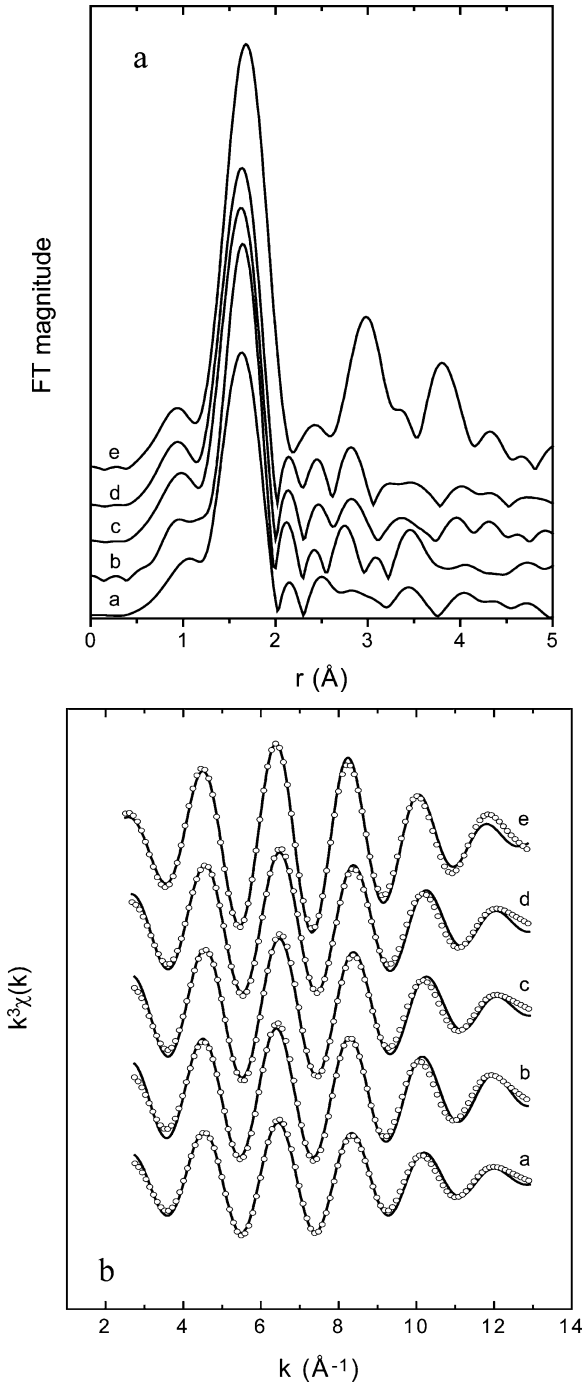

Fig. 10. EXAFS results for the catalysts. (a) Fourier transforms of $k^3\chi(k)$ spectra of the catalysts (same notation as in Fig. 9). The FTs were shifted vertically for sake of clarity; (b) filtered $k^3\chi(k)$ spectra (solid line) of the catalysts and the corresponding fit (open circles) with one shell of nearest O neighbors.

more ordered in the catalyst structure, with respect to that in the monoclinic lattice of Bi_2O_3.

The systematic increase of N, for the samples Bi4.26 to Bi6.64, shows a slight tendency of the Bi environment to be enriched with oxygen when Bi loading increases. This is most apparent for the sample Bi6.64, possibly related to the local formation of a crystalline compound around the Bi atoms.

Table 7
The nearest neighboring shell of the Bi atoms in the investigated catalysts

Sample	N	R (Å)	$\Delta\sigma^2$ ($\times 10^{-3}$ Å^2)
Bi4.26	2.4	2.20	−6
Bi5-wi	2.7	2.21	−7
Bi5-di	3.1	2.19	−6
Bi5.54	3.0	2.19	−6
Bi6.64	3.7	2.22	−7

N, number of the nearest neighbors (O atoms); R, Bi–O distance; $\Delta\sigma^2$, relative structural disorder of the nearest neighboring shell with respect to that in the standard compound α-Bi_2O_3 ($\Delta\sigma^2 = \sigma^2_{\text{catalyst}} - \sigma^2_{\text{standard}}$). The fit uncertainties in the values of N, R, and $\Delta\sigma^2$ are 0.7, 0.01, and 0.002 Å^2, respectively.

3.7. Catalytic behavior

Table 8 gives the catalytic performances of the investigated catalysts in the three oxidation reactions at 70 °C. The parent Na-ZSM-5 was completely inactive in oxidation of the investigated organic substrates and only nonselective H_2O_2 decomposition was observed. Protonic exchange of this sample resulted in a slight catalytic activity, but this was also accompanied by an enhanced H_2O_2 decomposition rate. Just like the parent Na-ZSM-5, the two Bi-impregnated ZSM-5 samples (Bi5-wi and Bi5-di) prepared by postsynthe-

Table 8
Catalytic properties of ZSM-5 samples at 70 °C

ZSM-5 sample	Hydrocarbon	Millimoles transformed hydrocarbon/ g catalyst[a]	Millimoles transformed H_2O_2/ g catalyst[a]	H_2O_2 efficiency (mol%)
Na-ZSM-5	Benzene	–	610	–
	Toluene	–	625	–
	Cyclohexane	–	625	–
H-ZSM-5	Benzene	8.4	1194	0.70
	Toluene	8.4	1194	0.82
	Cyclohexane	6.0	1194	0.70
Bi4.26	Benzene	124.8	980	12.7
	Toluene	214.2	1020	21.4
	Cyclohexane	204.1	990	41.2
Bi5.54	Benzene	168.1	1176	14.3
	Toluene	313.6	1188	35.5
	Cyclohexane	304.3	1188	51.2
Bi6.64	Benzene	19.6	1194	1.64
	Toluene	20.8	1188	2.17
	Cyclohexane	16.8	1194	2.81
Bi wet impregnation	Toluene	–	1164	–
Bi dry impregnation	Toluene	–	1068	–

[a] Reaction time 90 min.

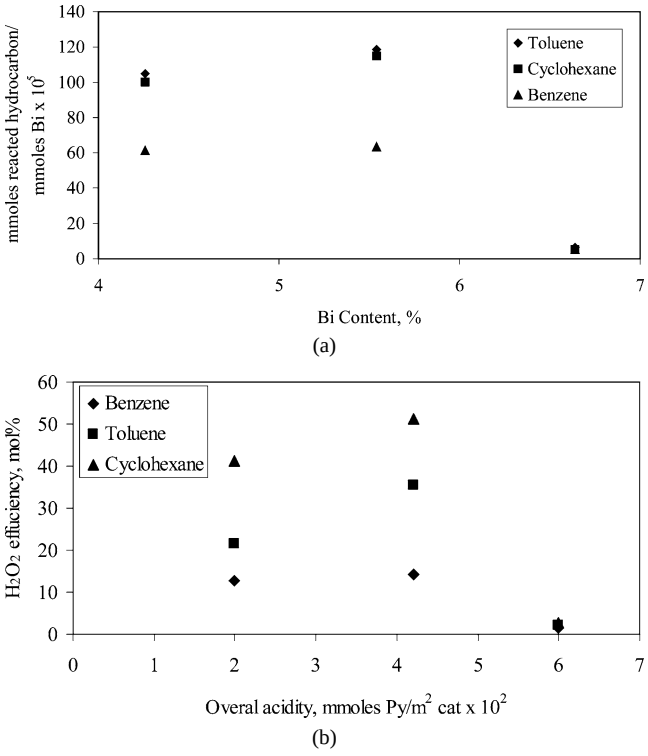

Fig. 11. Catalytic activity of the investigated samples (a) hydrocarbon conversion; (b) H_2O_2 efficiency (0.1 g catalyst, 120 mmol of hydrocarbon, H_2O_2 (30 wt% aqueous solution), hydrocarbon molar ratio of 1:1, 90 min, 70 °C, 1000 rpm). The acidity is measured by the total pyridine adsorption at 423 K.

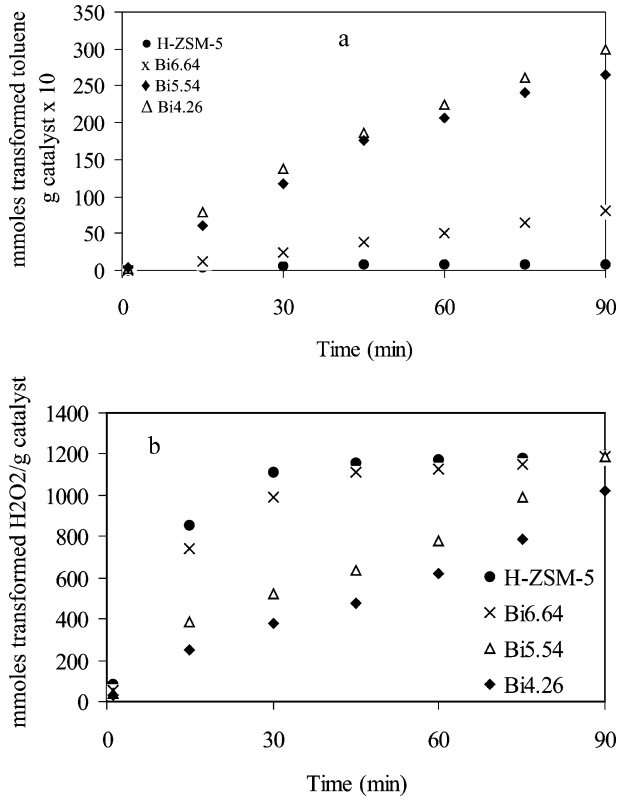

Fig. 12. Time dependence of the catalytic activity (a) hydrocarbon conversion; (b) H_2O_2 conversion (H_2O_2 (30 wt% aqueous solution), hydrocarbon molar ratio of 1:1, 70 °C, 1000 rpm).

sis routes led only to the nonselective H_2O_2 decomposition. The presence of Bi in these impregnated catalysts increased, however, the decomposition rate significantly, as compared to Na-ZSM-5.

The occlusion of Bi in the ZSM-5 matrix induced an increase in catalytic activity with respect to toluene, benzene, and cyclohexane oxidation. The results in Fig. 11a indicate an almost constant hydrocarbon oxidation activity per Bi atom for the Bi4.26 and Bi5.54 catalysts which show only well-dispersed occluded Bi, and an almost zero activity for Bi6.64 which was shown to contain (just like the impregnated catalysts) highly segregated Bi oxides. It seems thus that the catalytic activity in hydrocarbon oxidation is essentially associated with grafted-occluded oxidic Bi species. Fig. 11b illustrates the variation in H_2O_2 efficiency (essentially determined by the rate of hydrogen peroxide decomposition) with the overall acidity expressed in millimole pyridine adsorbed at 150 °C per unit surface area of the catalyst. Fig. 11 displays no simple correlation between H_2O_2 decomposition rate and the density of acid sites. This lack of a correlation suggests that even though the high decomposition activity of H-ZSM-5 (Table 8) points to the Brönsted acid as the active site, some other catalytic decomposition site is introduced upon introduction of Bi oxidic phase.

A typical example of time dependence of the hydrocarbon and hydrogen peroxide conversion is given in Fig. 12. These data confirmed the effect of zeolite and bismuth content. ZSM-5 and Bi6.64 readily decomposed H_2O_2 (Fig. 12b) even though they did contain the same kind of sites (see Table 6) and this had as a direct effect a small hydrocarbon oxidation rate. An opposite behavior was observed for Bi4.26, which showed a lower H_2O_2 decomposition rate and a higher hydrocarbon conversion.

Fig. 13 shows the variation in the number of moles converted per mole of Bi after a 90-min reaction as a function of temperature. Bi.6.64 displays a very low activity over the investigated temperature range. For the other two catalysts, activities normalized per Bi atom were essentially the same and increasing the temperature led to a moderate increase in conversion.

The change in the substrate:H_2O_2 ratio from 1:1 to 3:1 led to a better efficiency of H_2O_2 but to a smaller conversion of the hydrocarbon.

The effect of the catalyst on the selectivity is only reported for the oxidation of toluene, because in the case of benzene and cyclohexane the selectivities were very high. For benzene, phenol was the only reaction product, and for cyclohexane, cyclohexanone was obtained with a high selectivity (98–99%) for all the Bi-ZSM-5 samples. For H-ZSM-5, cyclohexanol and cyclohexanone were formed in comparable proportions (cyclohexanol/cyclohexanone molar ratio of 1.5 at 70 °C).

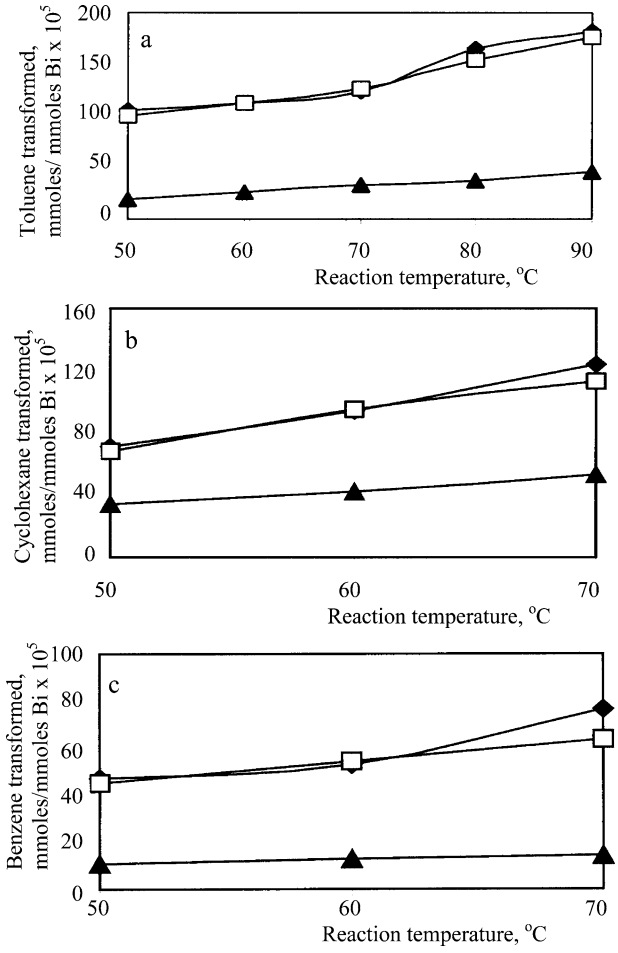

Fig. 13. Catalytic activity as function of temperature. (a) Toluene, (b) cyclohexane, (c) benzene (0.1 g catalyst, 120 mmol of hydrocarbon, H_2O_2 (30 wt% aqueous solution/hydrocarbon molar ratio of 1:1, 90 min, 1000 rpm). (◆) Bi4.26, (□) Bi5.54, and (▲) Bi6.64.

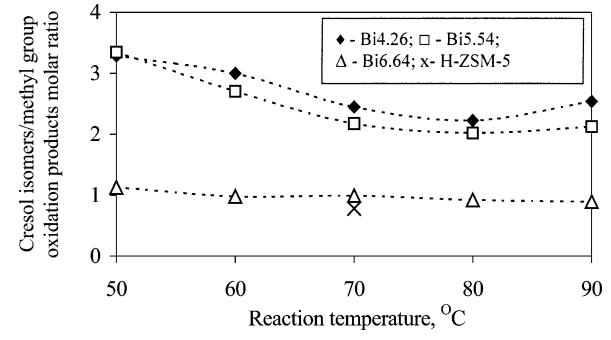

Fig. 14. Cresol isomers-to-methyl group oxidation in the toluene oxidation products as a function of temperature (0.1 g catalyst, 120 mmol of hydrocarbon, H_2O_2 (30 wt% aqueous solution/hydrocarbon molar ratio of 1:1, 90 min, 1000 rpm).

Fig. 14 shows the ratios of the cresol isomers to methyl group oxidation products, namely benzylic alcohol, benzaldehyde, and benzylic acid for the various temperatures investigated. For Bi6.64 the ratio was near 1, and the selectivity remained almost unchanged with temperature. For the other two catalysts, Bi4.26 and Bi5.54, the oxidation occurred merely at the aromatic ring, as the cresols were the dominant products. Increasing the temperature caused a slight decrease in the selectivity to cresols. Fig. 15 shows the distribution of the methyl oxidation group products on these catalysts. Bi.4.26 led only to benzylic alcohol. Increasing the Bi content resulted in an increased secondary oxidation to both benzaldehyde and benzoic acid.

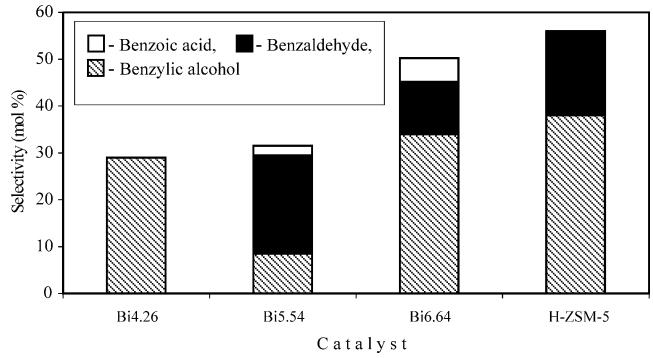

Fig. 15. Selectivity of the methyl group oxidation products of toluene (0.1 g catalyst 120 mmol of hydrocarbon, H_2O_2 (30 wt% aqueous solution/hydrocarbon molar ratio of 1:1, 90 min, 70 °C, 1000 rpm).

Analysis of the mother liquor separated by filtration at the reaction temperature indicated that Bi was not detected at the detection limit of ca. 10 ppm. If Bi was present at a lower concentration, it did not have any significant effect on the reaction rate.

4. Discussion

The characterization made on Bi-ZSM-5 samples obtained by direct synthesis suggested that Bi exists as Bi oxide clusters occluded in the ZSM-5 pores. Increasing the Bi content to 6.64 wt% led to the partial disruption of the ZSM-5 matrix and the formation of new phases. In this case, part of Bi seems to be segregated on the external surface. For Bi4.46 and Bi5.54, the clusters caused a deformation of the cell that was observed from the lower crystallinity as compared to the parent Na-ZSM-5. However, for these zeolites the amount of Bi was not sufficient to disrupt entirely the zeolite framework.

The development of Bi cluster phases in these zeolites may also be deduced from the pore blockage with increasing Bi concentration. FTIR investigation showed the presence of a band which may be ascribed to a Si–O–Bi bond. An increased tendency to enhance agglomeration with increasing Bi content was also inferred from the XPS and EXAFS data.

The way in which these Bi oxide clusters are generated may be deduced from the synthesis mechanism of these materials. The Bi^{3+} isolated cations are stable only in extremely acidic media (pH near 0) [111]. This condition was not fulfilled neither for the starting synthesis gels nor for the bismuth nitrate solution used for impregnation. Therefore, under the experimental synthesis conditions, oligomeric colloidal combinations, that may be formed by association of

BiO^+ or $[BiOH]^{2+}$, are rather favored. Studies concerning polynuclear oxocations of Bi indicated that the most abundant cation is $[Bi_6O_4(OH)_4]^{6+}$ [112].

Based on the characterization results it may be speculated that the crystallization process occurs by occlusion of the preformed bismuth oxide clusters in the growing ZSM-5 crystals. However, large cations such as octahedral $[Bi_6O_4(OH)_4]^{6+}$ units cannot be accommodated within the ZSM-5 channels. Therefore, as indicated by EXAFS, these cations can be split. Depending on the size of these clusters, the zeolite lattice may suffer damage at the BiO_x–SiO_2 boundary regions, resulting either in the creation of some defects (as shown by FTIR) or in a partial decrease of the crystallinity (as illustrated by XRD and FTIR measurements).

IR spectra of adsorbed pyridine showed that the introduction of Bi during the hydrothermal synthesis generated a specific acidity, consisting in weak Lewis sites and strong Brönsted sites. The Lewis acid sites may have originated in the coordinatively unsaturated bismuth cations in the bismuth oxide clusters and aluminum cations. Usually, bulky Bi_2O_3 is known as a nonstoichiometric oxide with an excess of oxygen anions, and basic character. Our results suggest that when clusters are present in a silicalite matrix, bismuth oxide changes its nonstoichiometry toward oxygen vacancies, even for a bismuthyl $(BiO)^+$-based structure. EXAFS comparative data on bismuth oxide and Bi-ZSM-5 zeolites sustain such an assumption. Indeed based on EXAFS data, increasing the bismuth oxide content led to an increased Bi coordination number N.

Brönsted acid sites associated to Bi might result from the condensation mechanisms [111] during the synthesis. One such mechanism is oxolation which involves condensation with water elimination:

$$(Bi_nO_{n-x}H_x)\text{–}OH + HO\text{–}\underset{|}{\overset{|}{Si}}\text{–} \overset{-H_2O}{\rightleftarrows} (Bi_nO_{n-x}H_x)\text{–}\underset{|}{\overset{|}{O}}\text{–}Si. \quad (1)$$

Another reaction could be olation, which corresponds to condensation by addition:

$$(Bi_nO_{n-x}H_x\text{–}BiO) + HO\text{–}\underset{|}{\overset{|}{Si}}\text{–}$$

$$\rightleftarrows (Bi_nO_{n-x}H_x)\text{–}BiO\diagdown\!\!\diagup \underset{H}{O} \diagdown\!\!\diagup \underset{|}{\overset{|}{Si}}\text{–}. \quad (2)$$

It is obvious from reactions (1) and (2) that the oxolation mechanism is favored by a hydroxo structure, while the olation occurs for the "oxo" precursors. Our results suggest that an oxo $(BiO)^+$ pathway is more probable, since the resulting –(BiO)···(HOSi) structures are expected to exhibit a stronger Brönsted acidity. Labilization of the H–O silanol bond occurs in this case as a contribution of the oxygen coordination electrons pair of the bismuthyl cation. The concentration of the Brönsted acid sites associated to boundary Bi–O–Si is expected to increase with growing bismuth content, if the dispersion level of the bismuth oxide clusters remains unchanged. The observed differences in acidity for these zeolites suggest that this is controlled by both the bismuth content and the size of these clusters.

Another explanation for the observed differences in the acidity of Bi-ZSM-5 catalysts may result from considering a charge compensation effect of positively charged BiO clusters. However, irrespective of the source of acidity, namely the Bi–O–Si bond formation or the charge compensation effect, this is caused by the presence of Bi, and the intensity is determined by its content.

For the Bi-impregnated ZSM-5 samples, Bi deposition occurs on the external surface with pore blocking. Almost no pyridine adsorption was evidenced by IR measurements. This behavior implies that the intrinsic acidity of the occluded bismuth oxide clusters is indeed related to the hydrothermal synthesis process of the zeolite.

CO_2-FTIR spectra indicated that these samples exhibited no basicity.

The catalytic activity of Bi-ZSM-5 samples is the direct consequence of the occlusion of the oxide clusters in the silica matrix. Both hydrothermal synthesis and impregnation led to some pore blockage. These are logically accomplished by mass transfer limitations. Remarkably, for Bi-ZSM-5 samples, the activity (expressed as moles hydrocarbon transformed per mole Bi) was higher than that generally reported for titanium silicalites [42,113–116]. Unfortunately, the H_2O_2 decomposition proceeds over these catalysts above the satisfactory limits, and much below the performances reported for titanium silicalites. There may be several reasons for this high decomposition rate. In titanium silicalites it has been shown that sodium ions [42] and even surface silanols [45] are detrimental to the selective use of H_2O_2. Moreover, even though TS-1 catalysts show some weak acid centers [14], they are usually limited in concentration due to the high Si/Ti ratios of these solids [113,114]. Here the support bears a Si/Al ratio close to 30 and a Al/Na ratio close to one. In addition, the acidity introduced by the occlusion of the Bi clusters may also be affecting the H_2O_2 decomposition rate. In the case of titanium-containing zeolites, the presence of extraframework TiO_2 also strongly decreases the hydrogen peroxide efficiency, which is comparable especially to Bi6.64 catalyst.

Oxidation of the various hydrocarbons investigated involves a different route. For benzene and for the aromatic ring of toluene, hydroxylation is catalyzed by the interaction with electrophilic oxygen species [54,116,117]. The oxidation of the methyl group of toluene, as well as the oxidation of cyclohexane, also involves a radical mechanism that determines their oxy-functionalization [118]. However, these mechanisms are both initiated on the Bi surface.

Bi sites seem to be obviously involved in hydroxylation of the aromatic ring, and a H_2O_2 activation through BiOOH electrophilic species could be assumed. A major contribution of acid sites in shifting the selectivity of toluene oxidation to the methyl group could be considered. This could

be related to the initiation of some radical pathways by acid sites, as previously suggested by Dai and Lunsford [119].

The high selectivity to cyclohexanone over Bi-ZSM-5 samples shows that the contribution of Bi sites is decisive for the secondary transformation of cyclohexanol, which is formed as an intermediate product. The redox properties of BiO_x clusters could be involved as follows,

$$C_6H_{11}OH + -\overset{\uparrow}{Bi}^{III}=O \rightarrow C_6H_{10}=O + -Bi^{II}=O + H^+,$$
$$\underset{\uparrow}{\quad\quad} H_2O_2 \underset{\quad\quad}{\quad\quad}$$

where the regeneration of oxidized Bi sites is ensured by the H_2O_2 consumption.

5. Conclusions

A series of bismuth oxides clusters occluded in a ZSM-5 matrix was obtained by hydrothermal treatment. For comparison, samples obtained via impregnation were also synthesized. The presence of Bi clusters in Bi4.26 and Bi5.54 was confirmed by EXAFS. Textural properties and crystallinity of the hydrothermally synthesized Bi-ZSM-5 depended on the Bi content. The characterization data collected from textural, XRD, XPS, and EXAFS of these zeolites showed that up to near 6 wt% Bi clusters were occluded in the ZSM-5 pores without major damages to the MFI structure. Higher loadings caused both framework damage and phase segregation. IR spectroscopy allowed illustration of the bismuth influence in disturbing the zeolite lattice and creating silanolic defects. In the presence of adsorbed pyridine, an intrinsic acidity of the bismuth oxides clusters was established. This consisted in weak Lewis sites that were attributed to coordinatively unsaturated bismuth or bismuthyl cations, and strong Brönsted sites, which were attributed to boundary Bi–O–Si linkages or a charge-compensating effect caused by positively charged BiO clusters.

Catalytic tests in liquid-phase oxidation of benzene, toluene, and cyclohexane using hydrogen peroxide as oxidizing agent showed that these catalysts are more active than the reported titanium silicalites. Unfortunately, the efficiency of H_2O_2 use was quite small, an important part of this being nonselectively decomposed. Several factors may contribute to this behavior such as the existence of Na species, the acidity, and the formation of large BiO clusters. The corroboration of all these data led to the conclusion that only very small clusters are effective in this reaction.

References

[1] M. Taramasso, G. Perego, B. Notari, US patent 4,410,501, 1983.
[2] B. Kraushaar, J.H.C. van Hooff, Catal. Lett. 2 (1989) 43.
[3] A.J.H.P. van der Pol, J.H.C. van Hoof, Appl. Catal. A 92 (1992) 93.
[4] A. Tuel, Y. Ben Taarit, Zeolites 13 (1993) 357.
[5] A. Tuel, Y. Ben Taarit, Zeolites 14 (1994) 594.
[6] A. Thangaraj, R. Kumar, S.P. Mirajkar, P. Ratnasamy, J. Catal. 130 (1991) 1.
[7] A. Tuel, Y. Ben Taarit, J. Chem. Soc., Chem. Commun. (1994) 1667.
[8] A. Carati, S. Contarini, R. Millini, G. Bellussi, Mat. Res. Soc. Ext. Abstr. (EA-24) (1990) 47.
[9] R. de Ruiter, J.C. Jansen, H. Van Bekkum, in: M.L. Occelli, H.A. Robson (Eds.), Molecular Sieves, van Nostrand–Reinhold, Princeton, NJ, 1993, p. 167.
[10] J.M. Popa, J.L. Guth, H. Kessler, Eur. patent 292,363, 1988.
[11] J.L. Guth, H. Kessler, J.M. Higel, L.M. Lamblin, J. Patarin, A. Seive, J.M. Chezeau, R. Wey, in: M.L. Occelli, M.A. Robson (Eds.), Zeolite Synthesis, in: ACS Symp. Ser., Vol. 398, 1989, p. 176.
[12] Q. Shilun, P. Wenqin, Y. Shangqing, Stud. Surf. Sci. Catal. A 49 (1989) 133.
[13] A. Lopez, M.H. Tuiler, H. Kessler, J.L. Guth, L. Delmotte, J.M. Popa, J. Solid State Chem. 102 (1993) 480.
[14] A. Bittar, A. Sayari, S. Kaliaguine, Res. Chem. Interm. 18 (1992) 49.
[15] G. Bellussi, A. Carati, M.G. Clerici, A. Esposito, R. Millini, F. Buonomo, Belg. patent 1,001,038, 1989.
[16] J.S. Reddy, R. Kumar, P. Ratnasamy, Appl. Catal. A 58 (1990) L1.
[17] H. Fu, S. Kaliaguine, J. Catal. 148 (1994) 540.
[18] J.E. Gallot, H. Fu, M.P. Kapoor, S. Kaliaguine, J. Catal. 161 (1996) 798.
[19] M.A. Camblor, A. Corma, J. Perez-Pariente, J. Chem. Soc., Chem. Commun. (1993) 557.
[20] T. Blasco, M.A. Camblor, A. Corma, J. Perez-Pariente, J. Am. Chem. Soc. 115 (1993) 11806.
[21] J.S. Reddy, A. Sayari, J. Chem. Soc., Chem. Commun. (1995) 23.
[22] C. Ferrini, H.W. Kouvenhoven, in: Proc. DGMK Conf. Selective Oxidations in Petrochemistry, Goslar, Germany (September 1992), 1992, p. 205.
[23] US patent 08/32,97,32, to ARCO Chemical Technology, L.P.
[24] C.B. Dartt, M.E. Davis, Appl. Catal. A 143 (1996) 53.
[25] C.T. Kresge, M.E. Leonowicz, W.J. Roth, J.C. Vartuli, J.S. Beck, Nature 359 (1992) 710.
[26] A. Corma, M.T. Navarro, J. Perez-Pariente, F. Sanchez, Stud. Surf. Sci. Catal. 84 (1994) 69.
[27] P.T. Tanev, M. Chibwe, T.J. Pinnavaia, Nature 368 (1994) 321.
[28] T. Blasco, A. Corma, M.T. Navarro, J. Perez-Pariente, J. Catal. 156 (1995) 65.
[29] Z. Liu, Diss. Abstr. Int. 57 (1996) 1256.
[30] W. Zhang, T.J. Pinnavaia, Catal. Lett. 38 (1996) 261.
[31] M. Dusi, T. Mallat, A. Baiker, J. Mol. Catal. 138 (1999) 15.
[32] D. Trong On, M.P. Kapoor, S. Kaliaguine, J. Chem. Soc., Chem. Commun. (1996) 1161.
[33] D. Trong On, M.P. Kapoor, P.N. Joshi, L. Bonneviot, S. Kaliaguine, Catal. Lett. 44 (1997) 171.
[34] G. Perego, G. Bellussi, C. Corno, M. Taramasso, F. Buonomo, A. Esposito, Stud. Surf. Sci. Catal. 28 (1986) 129.
[35] B. Notari, Stud. Surf. Sci. Catal. 37 (1988) 413.
[36] R. Millini, E. Previde-Massara, G. Perego, G. Bellussi, J. Catal. 137 (1992) 497.
[37] M.R. Boccuti, K.M. Rao, A. Zecchina, G. Leofanti, G. Petrini, Stud. Surf. Sci. Catal. 48 (1989) 133.
[38] G. Bellussi, A. Carati, M.G. Clerici, G. Maddinelli, R. Millini, J. Catal. 133 (1992) 220.
[39] D.R.C. Huybrechts, P.L. Buskens, P.A. Jacobs, J. Mol. Catal. 71 (1992) 129.
[40] J.E. Gallot, D. Trong On, M.P. Kapoor, S. Kaliaguine, IEC Res. 36 (1997) 3458.
[41] J.E. Gallot, M.P. Kapoor, S. Kaliaguine, AIChE J. 44 (1998) 1438.
[42] J.E. Gallot, S. Kaliaguine, Can. J. Chem. Eng. 76 (1998) 833.
[43] S.M. Kuznicki, US patent 4,938,939, 1990.
[44] M. Deeba, C.F. Keweshan, G.S. Koermer, S.M. Kuznicki, R.S. Madon, in: J.R. Kosak, T.A. Johnson (Eds.), Catalysis of Organic Reactions, Dekker, New York, 1994, p. 383.
[45] D. Trong On, M.P. Kapoor, E. Thibeault, J.E. Gallot, G. Lemay, S. Kaliaguine, Micropor. Mater. 20 (1998) 107.
[46] M. Anpo, H. Nakaya, S. Kodama, Y. Kubokawa, J. Phys. Chem. 90 (1986) 1633.

[47] A. Fernandez, J. Leyrer, A.R. Gonzalez-Felipe, G. Munuera, H. Knozinger, J. Catal. 112 (1988) 489.
[48] G. Petrini, A. Cesana, G. De Alberti, F. Genoni, G. Leofanti, M. Padovan, G. Paparatto, P. Roffia, Stud. Surf. Sci. Catal. 68 (1991) 761.
[49] A. Tuel, Y. Ben Taarit, Micropor. Mater. 1 (1993) 179.
[50] R. Hari Prasad, A.V. Ramaswamy, Appl. Catal. 93 (1993) 123.
[51] R. Neumann, M. Levin-Elad, Appl. Catal. 122 (1995) 85.
[52] Y.-W. Chen, Y.-H. Lu, Ind. Eng. Chem. Res. 38 (1999) 1893.
[53] N.K. Mal, A.V. Ramaswamy, J. Mol. Catal. 105 (1996) 149.
[54] N.K. Mal, A.V. Ramaswamy, Appl. Catal. 143 (1996) 75.
[55] A.P. Singh, T. Selvam, J. Mol. Catal. 113 (1996) 489.
[56] S. Gontier, A. Tuel, Appl. Catal. 143 (1996) 125.
[57] Z. Zhang, J. Suo, X. Zhang, S. Li, Appl. Catal. 179 (1999) 11.
[58] P. Ratnasamy, R. Kumar, in: L. Bonneviot, S. Kaliaguine (Eds.), Zeolites—A Refined Tool for Designing Catalytic Sites, in: Stud. Surf. Sci. Catal., Vol. 97, Elsevier, Amsterdam, 1995, p. 367.
[59] L. Davies, P. McMorn, D. Bethell, Ph.C. Bulman Page, F. King, F.E. Hancook, G.J. Hutchings, Chem. Commun. (2000) 1807.
[60] T. Yashima, Y. Kobayashi, T. Komatsu, S. Namba, in: L. Guczi, et al. (Eds.), New Frontiers in Catalysis, Elsevier, Amsterdam, 1993, p. 1689.
[61] T. Yashima, S. Nagase, T. Komatsu, S. Namba, in: T. Inui, et al. (Eds.), New Aspects of Spillover Effect in Catalysis, Elsevier, Amsterdam, 1993, p. 417.
[62] A. Bielanski, J. Haber, Oxygen in Catalysis, Elsevier, Amsterdam, 1991.
[63] T. Mallat, A. Baiker, Catal. Today 19 (1994) 247.
[64] M. Besson, P. Gallezot, Catal. Today 57 (2000) 127.
[65] M. Wenkin, C. Renard, P. Ruiz, B. Delmon, M. Devillers, Stud. Surf. Sci. Catal. 110 (1997) 181.
[66] H. Kimura, K. Tsuto, T. Wakisaka, Y. Kazumi, Y. Inaya, Appl. Catal. A 96 (1993) 217.
[67] T. Tsujino, S. Ohigashi, S. Sugiyama, K. Kawashiro, H. Hayashi, J. Mol. Catal. 71 (1992) 25.
[68] F. Alardin, P. Ruiz, B. Delmon, M. Devillers, Appl. Catal. A 215 (2001) 125.
[69] A. Abbadi, H. Van Bekkum, Appl. Catal. A 124 (1995) 409.
[70] A. Abbadi, K.F. Gotlieb, J.B.M. Meiberg, H. Van Bekkum, Appl. Catal. A 156 (1997) 105.
[71] T. Mallat, Z. Bodnar, A. Baiker, O. Greis, H. Sturbig, A. Reller, J. Catal. 142 (1993) 237.
[72] P. Fordham, M. Besson, P. Gallezot, Catal. Lett. 46 (1997) 195.
[73] A. Abbadi, H. Van Bekkum, Appl. Catal. A 148 (1996) 113.
[74] E.M. Flanigen, Nature 271 (1978) 437.
[75] M. Padovan, Zeolites 4 (1984) 295.
[76] J.J. Rehr, J. Mustre de Leon, S.I. Zabinsky, R.C. Albers, J. Am. Chem. Soc. 113 (1991) 5135.
[77] J. Mustre de Leon, J.J. Rehr, S.I. Zabinsky, R.C. Albers, Phys. Rev. B 44 (1991) 4146.
[78] M.M. Treacy, J.B. Higgins, R. Von Ballmoos, Collection of Simulated XRD Powder Patterns for Zeolites, 3rd rev. ed., Elsevier, New York, 1996.
[79] G. Debras, A. Gourgue, J.B. Nagy, G. De Clippeleir, Zeolites 5 (1985) 369.
[80] E.G. Derouane, S. Detremmerie, Z. Gabelica, N. Blom, Appl. Catal. A 1 (1981) 201.
[81] G. Giannetto, R. Monque, J. Perez, J. Papa, L. Garcia, Zeolites 13 (1993) 557.
[82] G. Giannetto, R. Monque, J. Papa, J. Perez, L. Garcia, Z. Gabelica, Zeolites 14 (1994) 549.
[83] A. Araya, B.M. Lowe, Zeolites 6 (1986) 111.
[84] X. Liu, J. Klinowski, J. Phys. Chem. 96 (1992) 3403.
[85] H. Kosslik, V.A. Tuan, B. Parlitz, R. Frike, C. Peuker, W. Storek, J. Chem. Soc., Faraday Trans. 89 (1993) 1131.
[86] B.F. Mentzen, M. Sacerdot-Peronnet, J.-F. Berar, F. Lefebvre, Zeolites (1993) 485.
[87] International Tables for X-Ray Crystallography, Vol. III, Physical and Chemicals Tables, The Kynoch Press, Birmingham, 1962.
[88] V.S. Dharmadhikari, S.R. Sainkar, S. Badrinarayan, A. Goswami, J. Electron. Spectr. Relat. Phenom. 25 (1992) 181.
[89] E.M. Flanigen, H. Khatami, H.A. Szymanski, Adv. Chem. Ser. 101 (1971) 201.
[90] E. Astorino, J.B. Peri, R.J. Willey, G. Busca, J. Catal. 157 (1995) 482.
[91] R. Szostak, V. Nair, J. Chem. Soc., Faraday Trans. 83 (1987) 487.
[92] R.A. Le Febre, J.C. Jansen, H. van Bekkum, Zeolites 7 (1987) 471.
[93] K.H. Rhee, U.S. Rao, J.M. Stencel, G.A. Melson, J.E. Crawford, Zeolites 3 (1983) 387.
[94] R.B. Borade, A. Sayari, A. Adnot, S. Kaliaguine, J. Phys. Chem. 94 (1990) 5989.
[95] L.N. Malashevich, Ya.B. Tsybul'skaya, A.D. Borisevich, Kinet. Katal. 18 (1977) 1599.
[96] M. Ai, T. Ikawa, J. Catal. 40 (1975) 203.
[97] D.G. Rethwisch, J.A. Dumesic, Langmuir 2 (1986) 73.
[98] G. Herzberg, Infrared and Raman Spectra of Polyatomic Molecules, Van Nostrand, New York, 1947, p. 274.
[99] A. Zecchina, S. Coluccia, E. Guglielminotti, G.J. Ghiotti, Phys. Chem. 75 (1971) 2790.
[100] J.B. Peri, J. Phys. Chem. 70 (1966) 3068.
[101] J. Vilckova, J. Barton, Chem. Commun. 9 (1973) 306.
[102] J.W. Ward, A.V. Habgood, J. Phys. Chem. 70 (1966) 1178.
[103] G. Ramis, G. Busca, C. Cristiani, L. Lietti, P. Forzatti, F. Bregani, Langmuir 8 (1992) 1744.
[104] E. Guglielminotti, L. Cerruti, E. Borello, Gazz. Chim. Ital. 107 (1977) 447.
[105] R.P. Einschens, W.A. Pliskin, Adv. Catal. 9 (1966) 1431.
[106] Y. Kozirovski, M. Folman, Trans. Faraday Soc. 62 (1966) 1431.
[107] K. Yamada, W.B. Pearson, J. Chem. Phys. 41 (1964) 2748.
[108] H. Knozinger, Adv. Catal. Related Subj. 25 (1976) 184.
[109] H.A. Harwig, Z. Anorg. Allg. Chem. 444 (1978) 151.
[110] T.A. Carlson, C.W. Nestor Jr., T.C. Tucker, F.B. Malik, Phys. Rev. 169 (1968) 27.
[111] J. Livage, M. Henry, C. Sanchez, Prog. Solid State Chem. 18 (1988) 259.
[112] B. Sundrall, Acta Chem. Scand. Ser. A 33 (1979) 219.
[113] A.V. Ramaswamy, S. Sivasanker, P. Ratnasamy, in: Symposium on New Catalytic Chemistry Utilizing Molecular Sieves, 206th Meeting (August 22–27, 1993), Division of Petroleum Chemistry, Inc., American Chemical Society, Chicago, 1993, p. 765.
[114] T. Tatsumi, K. Asano, K. Yanagisawa, in: J. Weitkamp, H.G. Karge, W. Hölderich (Eds.), Zeolites and Related Microporous Materials: State of the Art 1994, in: Stud. Surf. Sci. Catal., Vol. 84, Elsevier, Amsterdam, 1994, p. 1861.
[115] E.V. Spinacé, H.O. Pastore, U. Schuchard, J. Catal. 157 (1995) 631.
[116] B. Notari, in: Symposium on New Catalytic Chemistry Utilizing Molecular Sieves, 206th Meeting (August 22–27, 1993), Division of Petroleum Chemistry, Inc., American Chemical Society, Chicago, 1993, p. 761.
[117] R.A. Sheldon, J. Dakka, Catal. Today 19 (1994) 215.
[118] D.R.C. Huybrechts, P.L. Buskens, P.A. Jacobs, Nature 345 (1990) 240.
[119] P.S.E. Dai, J.H. Lunsford, J. Catal. 64 (1980) 184.